Rare Met. (2021) 40(10):2819–2828
https://doi.org/10.1007/s12598-021-01753-w

RARE METALS

ORIGINAL ARTICLE

Realizing high thermoelectric properties in p-type polycrystalline SnSe by inducing DOS distortion

Yu-Ping Wang, Bing-Chao Qin, Dong-Yang Wang, Tao Hong, Xiang Gao, Li-Dong Zhao*

Received: 10 February 2021 / Revised: 28 February 2021 / Accepted: 11 March 2021 / Published online: 26 May 2021

Abstract SnSe crystals have been discovered as one of the most efficient thermoelectric materials due to their remarkable thermal and electrical transports. But the polycrystalline SnSe possesses much lower performance especially for the low carrier mobility and electrical conductivity. We firstly attempted to explain and verify the difference in the electrical conductivity as a function of temperature between p-type crystalline and polycrystalline SnSe by considering the grain boundary effects in the polycrystalline samples. On the basis of 2% Na doping to optimize the carrier concentration, the carrier mobility is improved by further introducing In, leading to enhanced carrier mobility from 3 to 9 $cm^2 \cdot V^{-1} \cdot s^{-1}$ in polycrystalline SnSe. Moreover, In doping introduces extra resonant levels in SnSe, which increases the density of states near Fermi level and leads to an enhanced band effective mass. Large Seebeck coefficient of $\sim$ 205 $\mu V \cdot K^{-1}$ at 300 K and maximum power factor of $\sim$ 7.5 $\mu W \cdot cm^{-1} \cdot K^{-2}$ at 773 K can be obtained in the $Sn_{0.975}Na_{0.02}In_{0.005}Se$ sample, leading to a competitively high dimensionless figure of merit (*ZT*) value exceeding 1.1 at 773 K.

Keywords Thermoelectric; p-type polycrystalline SnSe; Carrier mobility; Resonant effect; Band effective mass

Supplementary Information The online version contains supplementary material available at https://doi.org/10.1007/s12598-021-01753-w.

Y.-P. Wang, B.-C. Qin, D.-Y. Wang, T. Hong, L.-D. Zhao*
School of Materials Science and Engineering, Beihang University, Beijing 100191, China
e-mail: zhaolidong@buaa.edu.cn

X. Gao
Center for High Pressure Science and Technology Advanced Research (HPSTAR), Beijing 100094, China

1 Introduction

Thermoelectric materials and technologies, which convert thermal energy to electricity, offer an alternative option of harvesting waste heat [1, 2]. The thermoelectric energy conversion efficiency of a given material is determined by the dimensionless figure of merit, $ZT = S^2\sigma T/(\kappa_{ele} + \kappa_{lat})$, where S is the Seebeck coefficient, σ is the electrical conductivity, T is the absolute temperature, κ_{ele} is the electronic thermal conductivity and κ_{lat} is the lattice thermal conductivity [1–4].

In the cause of optimizing the thermoelectric performance, expended efforts should be made to boost the power factor (PF = $S^2\sigma$) or decrease thermal conductivity [5–14]. Over the past decades, substantial strategies have been taken in the development of high *ZT* values, including carrier concentration engineering [15–18], band structure engineering [19–22] and all scale hierarchical architecturing [23, 24]. Alternatively, one could look for promising candidates with intrinsically low thermal conductivity, which mainly derives from anisotropic and anharmonic bonding [25], copper ion liquid-like behavior [26], and complex crystal structure [27–29], etc.

SnSe is a quasi-two-dimension-layered binary compound with an orthogonal structure. SnSe crystals have attracted extensive attention due to excellent thermoelectric properties and ultrahigh *ZT* values have been achieved in both p-type [30–33] and n-type SnSe crystals [34, 35]. However, crystal SnSe has the disadvantages of high cost, long term to prepare, poor mechanical properties, and thus hard for industrial application. So, polycrystalline SnSe has been attracting extensive attentions. To date, the polycrystalline SnSe system has also been greatly developed. Owing to the limitation of electrical conductivity and carrier mobility, the thermoelectric performance of

polycrystalline SnSe is not ideal, showing low *ZT* values [15, 17, 36–38]. Researches show that alkali metal doping can effectively control the carrier concentration while Na was confirmed as the most effective dopant, which can significantly improve the electrical transport properties [36, 39–44].

In has the ability to introduce extra valence state by forming In^{+} and In^{3+} simultaneously [45]. And former studies have shown that the Seebeck coefficient of In-doped SnTe can be greatly increased, because the resonant state improves the density of electronic states [46]. This inspires us to investigate whether In can form resonant level in SnSe system. In this work, we introduced small amounts of In on the basis of 2% Na doping as p-type dopant. Our results show that the simultaneously optimized carrier mobility and Seebeck coefficient can be achieved. Specifically, the carrier mobility was increased from ~ 3 to ~ 9 $cm^2 \cdot V^{-1} \cdot s^{-1}$, while a nearly 50% increase in the Seebeck coefficient was obtained at 300 K by In doping. In the full temperature range, both electrical conductivity and Seebeck coefficient are increased significantly, leading to greatly enhanced power factors approaching ~ 7.5 $\mu W \cdot cm^{-1} \cdot K^{-2}$ at 773 K. And the final *ZT* value shows an increase from ~ 0.64 to ~ 1.1 at 773 K. Besides, the comparison between crystalline and polycrystalline p-type SnSe of the electrical conductivity demonstrated in this work gives reasonable explanations on the three-stage trend of electrical conductivity curve of the polycrystalline SnSe by considering the grain boundary effects, which might be implemented for further performance enhancement of polycrystalline SnSe systems by grain boundary modification.

2 Experimental

The high-purity elements Sn, Se, Na and In were weighed according to the stoichiometric ratio $Sn_{0.98-x}Na_{0.02}In_xSe$ (x = 0%, 0.25%, 0.50%, 0.75% and 1.00%) under a glove box filled with nitrogen, put into carbon-coated quartz tube, and flame-sealed under vacuum below 1×10^{-2} Pa. The tubes were loaded into muffle furnace, slowly heated to 1223 K in 12 h, then kept for 12 h, cooled to 793 K in 6 h, kept for 12 h, and naturally cooled to room temperature. The obtained ingots were subsequently ground into powders and densified with spark plasma sintering (SPS-211Lx). Obtained compact cylindrical samples were then used to measure phases, electrical and thermal transport properties, microstructure characterizations, and Hall coefficients. Density functional theory (DFT) calculations were conducted to analyze electrical transport properties. The experimental details can be found in the Supporting Information (SI).

3 Results and discussion

3.1 Analysis of electrical conductivity of polycrystalline SnSe

The electrical conductivity of hole-doped SnSe crystal is shown in Fig. 1a, indicating a metallic conduction behavior as the electrical conductivity gradually decreases with temperature rising. This can be attributed to the enhanced acoustic-electric scattering (phonon-electron scattering) effect with high temperatures, and thus the carrier mobility declines, leading to a temperature dependency of electrical conductivity ($T^{-3/2}$) due to the dominated acoustic phonon scattering (APS) [47, 48]. Figure 1b shows the electrical conductivity of hole-doped polycrystalline SnSe. Different from the SnSe crystals, the electrical conductivity of polycrystalline SnSe can be divided into three parts. Below ~ 400 K, the electrical conductivity goes up as temperature increases, and then decreases at 400–650 K, showing typical semiconductor conducting characteristics, while experiences an upward process at the temperatures above 650 K.

The SnSe crystals were prepared by the vertical Bridgman method using tube furnace, and the crystal can be directly cut into bars for thermoelectric performance testing. However, for polycrystalline, it is necessary to crush the SnSe polycrystalline ingots and perform SPS. Figure 1c is a typical back-scattered electron (BSE) image, which shows the extensive grains processed by SPS, with a size of ~ 40 mm or lower, which means that the density of grain boundaries (GBs) has increased significantly during the synthesis of polycrystalline samples. At low temperatures, the grain boundary scattering is dominant, and the existence of extensive grain boundaries restricts the migration of carriers and limits the electrical conductivity [49, 50].

There are potential barriers that block the movement of charge carriers near the grain boundaries. Meanwhile, studies show that, compared with atoms inside the grain boundary, atoms at/near the interfaces between grain boundaries are in a disordered state. There are large numbers of incomplete atomic bonds, thus forming multiple defects [46], which can capture carriers (holes or electrons). As a result, the grain boundary is electrified and a grain boundary potential is formed, which adversely affects the electrical conductivity at low temperature. Phonon scattering dominates the interior of the grain

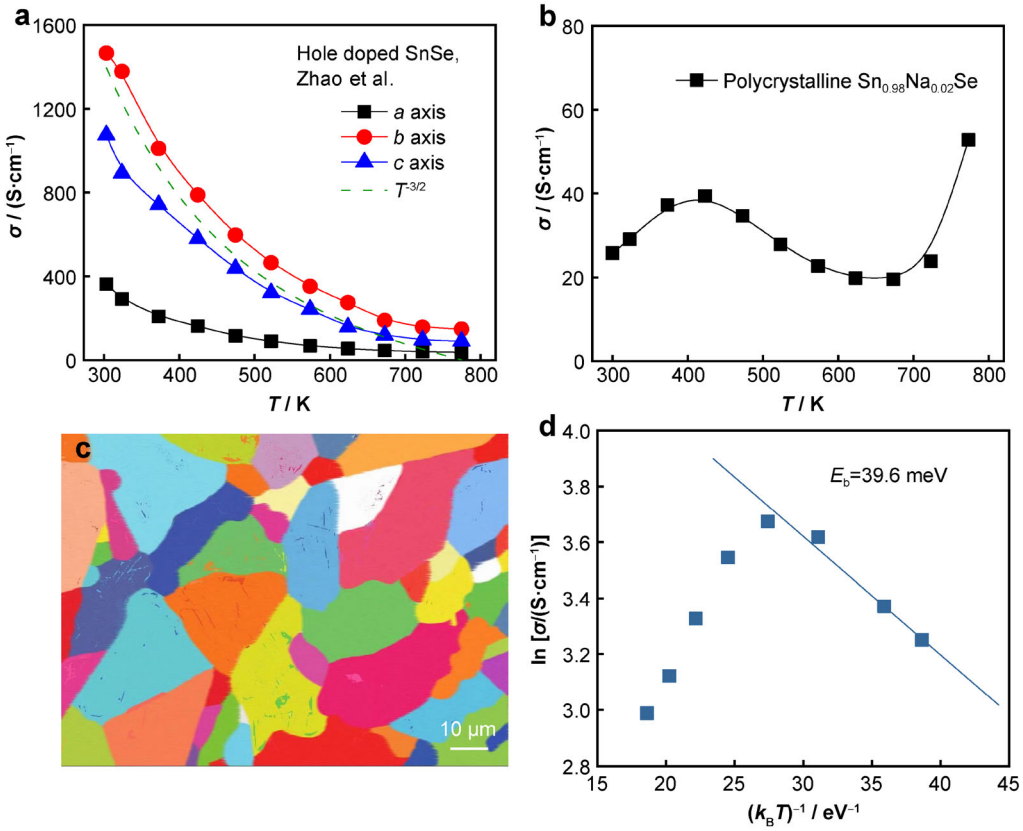

Fig. 1 Temperature dependent of electrical conductivity of **a** SnSe crystal [31] and **b** polycrystalline $Sn_{0.98}Na_{0.02}Se$; **c** back-scattered electron (BSE) image showing grains with various grain size of polycrystalline $Sn_{0.98}Na_{0.02}Se$; **d** relationship between lnσ and $(k_BT)^{-1}$ under dominant system of grain boundary scattering

boundary; however, due to the existence of the grain boundary barriers, the electrical conductivity at the grain boundaries (σ_{GB}) can be described as [51]:

$$\sigma_{GB} = e^2 \lambda n \left(\frac{1}{2\pi m k_B T}\right)^{1/2} \exp\left(\frac{-E_b}{k_B T}\right) \quad (1)$$

where e is the electron charge, λ is the grain size, n is the carrier concentration, m is the carrier effective mass, k_B is the Boltzmann constant, T is the temperature in Kelvin, and E_b is the grain boundary barrier in a single dimension. Among them, the grain boundary barrier (E_b) is described by the following formula:

$$E_b = \frac{e^2 Q_t^2}{8N\varepsilon} \quad (2)$$

where Q_t is the concentration of trap states at the GBs, ε is the dielectric constant, and N is the doping density. Equation (2) corresponds to the case where the carrier concentration greater than Q_t. Kuo et al. [52] believe that the material consists of the GB phase and bulk grain phase, so that the total electrical conductivity can be expressed by the following equation:

$$\sigma^{-1} = (1-\alpha)\sigma_G^{-1} + \alpha\sigma_{GB}^{-1} \quad (3)$$

where α is a constant and represents the fraction of GB phase. In the temperature range dominated by grain boundary scattering, when the resistance from GBs is strong enough, then the contribution of bulk grain phase to electrical conductivity is masked by GBs. Then σ_{GB} in Eq. (1) is approximately equal to the whole electrical conductivity. If the carrier concentration stays the same, plotting the relationship between lnσ and $1/k_BT$, according to Eq. (1), would produce a straight line with a slope of $-E_b$ [51]. Therefore, we select the polycrystalline sample $Sn_{0.98}Na_{0.02}Se$ for verification, as shown in Fig. 1d. As expected, lnσ and $1/k_BT$ are linear in the dominant phase of low-temperature grain boundary scattering, well verifying the above analysis. The linear fitting curve of the slope indicates that the energy barrier of the grain boundary is estimated to be $\sim$ 39.6 meV based on the slope. And former studies have shown that the material which has larger E_b value exhibits better semiconductor characteristics under the same conditions [53]. Based on above analysis, for the polycrystalline SnSe, we can consider that rationally preparing larger grained samples through heat treatment and texture strategy may be beneficial to eliminate the grain

boundary scattering and promote the electrical performance.

However, as temperature increases, more holes and electrons are thermally excited to cross the grain boundary barriers to participate in the electrical conduction, and the electrical conductivity gradually increases up to ~ 400 K [53]. At $T > 400$ K, phonon-electron scattering becomes the dominate scattering mechanism, and the electrical conductivity shows a negative temperature dependence, consistent with that in crystal SnSe.

The critical temperature point of the phase transition (*Pnma-Cmcm*) in SnSe is ~ 800 K, while it is worth noting that studies have found that there is a continuous phase transition process with a temperature span of 200 K before the critical transition temperature [54–56]. Generally, the higher the symmetry of the crystal structure is, the lower the anharmonicity is, the lower the scattering on the carriers is, and the higher the carrier mobility can be achieved. This continuous phase transition changes the crystal structure, which causes a significant increase in the carrier mobility at high temperatures [34]. On the other hand, the variable temperature Hall measurement found that the carrier concentration of SnSe will rise significantly at the temperature of above 700 K [32], mainly due to the thermal excitation of a small number of carriers. Based on the above two factors, the electrical conductivity of polycrystalline SnSe increases at the temperatures above ~ 650 K, as shown in Fig. 1b

3.2 Phase structure characterization

Powder X-ray diffraction (XRD) patterns of $Sn_{0.98-x}Na_{0.02}In_xSe$ are shown in Fig. 2a, from which all samples present single *Pnma* phase (PDF No. 53–0527). It can be completely dissolved with SnSe to form a single phase for the range of 0.25%–1.00% In concentration with no miscellaneous phase in XRD patterns. The lattice parameters of SnSe after In doping are calculated shown in Fig. 2b, showing that In doping does not obviously affect the lattice parameters of SnSe because of the similar ionic radius of Sn^{2+} and In^{+}/In^{3+}.

3.3 Electrical transport properties for polycrystalline $Sn_{0.98-x}Na_{0.02}In_xSe$

Figure 3a shows the electrical conductivity of $Sn_{0.98-x}Na_{0.02}In_xSe$ samples. It is observed that electrical conductivity of all samples shows the same three-stage trend in the full temperature range, which was well analyzed as demonstrated above. The electrical conductivity increases with In doping, reaching maximum value of ~ 40 $S{\cdot}cm^{-1}$ for the sample $x = 0.5\%$ at room temperature. The electrical conductivity can be calculated as:

$$\sigma = ne\mu = \frac{ne^2\tau}{m^*} \tag{4}$$

where μ is the carrier mobility, and τ is the relaxation time. It can be seen from Eq. (4) that electrical conductivity is directly proportional to the carrier mobility. In order to obtain the carrier concentration and carrier mobility at room temperature, we conducted the Hall measurement for all samples, as shown in Fig. 3b. With In doping fraction rising, the room-temperature carrier mobility fluctuatingly increases and reaches the highest value of ~ 9 $cm^2{\cdot}V^{-1}{\cdot}s^{-1}$ for the sample $x = 0.50\%$, almost 3 times higher than that of In-free sample. This also corresponds to the maximum room-temperature electrical conductivity when $x = 0.50\%$, as shown in Fig. 3a.

Figure 3c shows the temperature dependence of the Seebeck coefficient for all samples, demonstrating largely enhanced Seebeck coefficients by In doping due to the resonant effect and the increased electronic density of states, which will be discussed later. Specifically, the room-temperature Seebeck coefficient was increased from ~

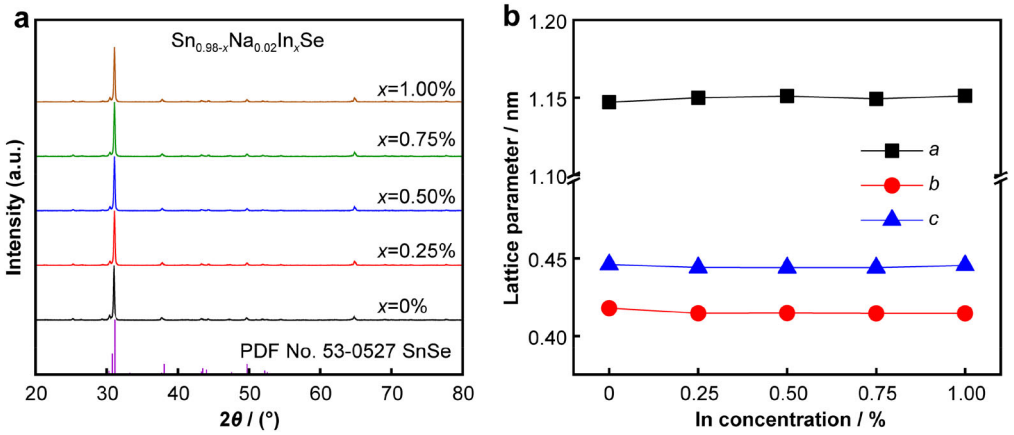

Fig. 2 **a** Powder XRD patterns and **b** lattice parameters of In-doped polycrystalline SnSe

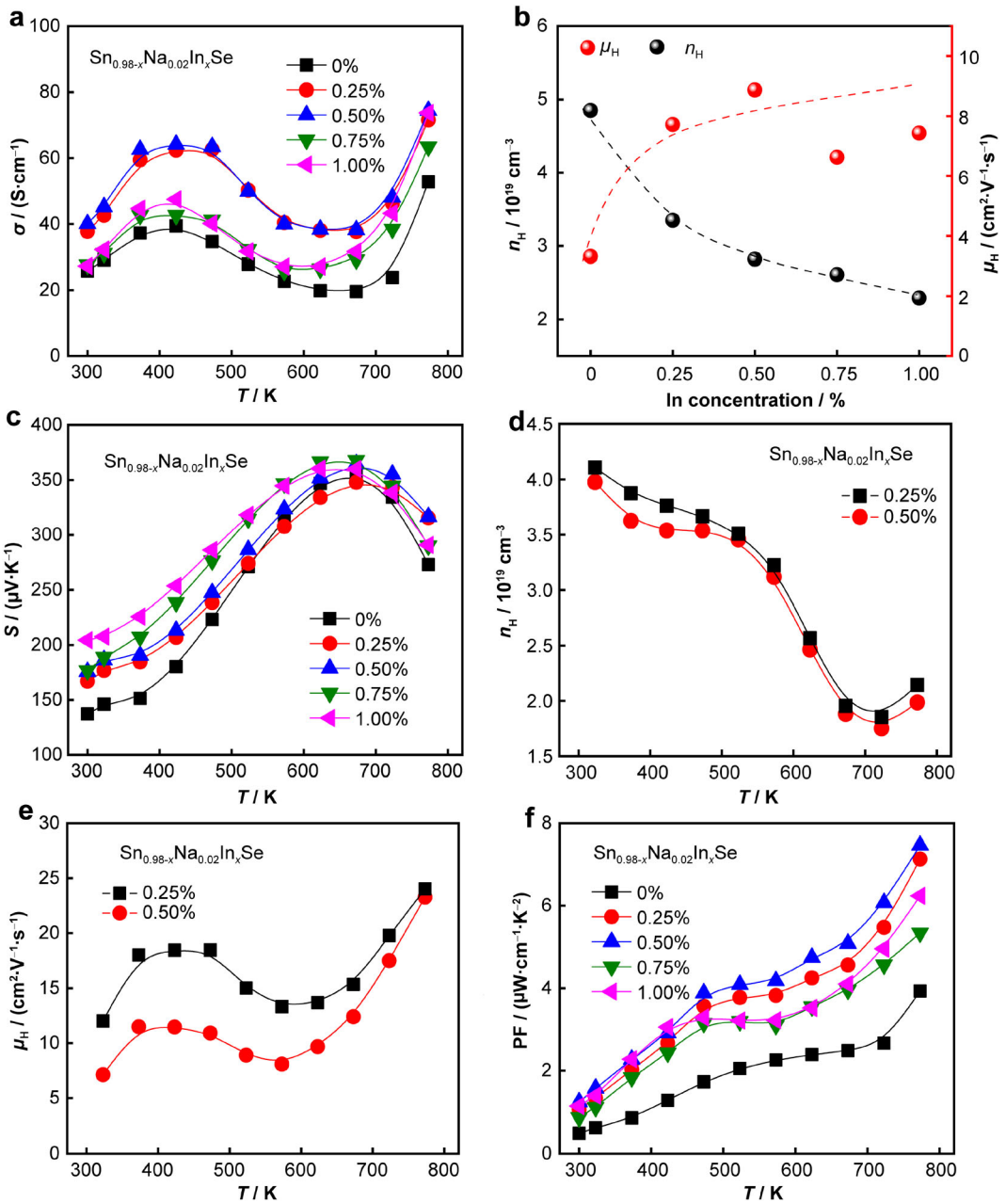

Fig. 3 Electrical transport properties of $Sn_{0.98-x}Na_{0.02}In_xSe$ samples with rising temperature: **a** electrical conductivity; **b** room temperature carrier concentration and carrier mobility; **c** Seebeck coefficient; **d** high-temperature carrier concentration; **e** high-temperature carrier mobility; **f** power factor

137 to ~ 205 $\mu V \cdot K^{-1}$ with In doping fraction increasing. The Seebeck coefficient increases with temperature rising, reaching a peak value around 700 K. At the temperatures above 700 K, the Seebeck coefficient decreases with temperature increasing. According to Eq. (5), the Seebeck coefficient is inversely proportional to the carrier concentration, so the decline of Seebeck coefficient above 700 K might arise from the increased carrier concentration due to the thermal excitation at high temperatures. To confirm this, we conducted the high-temperature Hall measurements for typical samples and found that the carrier concentration shows a similar upturn trend after 700 K, as shown in Fig. 3d, which is consistent with the downward trend of the Seebeck coefficient when $T > 700$ K. Moreover, the high-temperature Hall measurements and the calculated carrier mobility shown in Fig. 3e correspond to the electrical conductivity in Fig. 3a, further indicating the grain boundary effect and its influence on the electrical transport properties of polycrystalline SnSe as discussed above.

To investigate the effects on the Seebeck coefficient from In doping, we conducted first-principle calculations of the electronic band structure and density of state (DOS) for SnSe with and without In doping, as shown in Fig. 4. The Seebeck coefficient can be defined as:

$$S = \frac{8\pi^2\kappa_B^2}{3eh^2} m^* T \left(\frac{\pi}{3n}\right)^{\frac{2}{3}} \quad (5)$$

where m^* is the band effective mass, h is the Planck constant. The change of effective mass has a great influence on the Seebeck coefficient. Based on the electrical transport measurements at 300 K, the Pisarenko plot calculated by the single parabolic band (SPB) model is depicted in Fig. 4a with $m^* = 0.8m_0$ (m_0 is the mass of the electron) derived from the experimental data of the sample $x = 0$. The experimental data for In-doped samples locate much higher than the Pisarenko plot shown in Fig. 4a, indicating that the DOS effective increases with In doping in SnSe. In the meantime, based on the obtained band structures shown in Fig. 4c, d, the electronic density of states is calculated, as shown in Fig. 4b. Compared with the undoped sample, it is found that In doping can increase the integral of the energy near the Fermi level as the DOS curves become steeper, thereby improving the effective mass and producing a resonant state effect.

With the simultaneously optimized electrical conductivity and Seebeck coefficient by In doping in SnSe, the power factor as a function of temperature can be obtained in Fig. 3f. The power factor shows significant improvement over a wide temperature range after In doping, and the maximum value is increased from ~ 3.9 to ~ 7.5 $\mu W \cdot cm^{-1} \cdot K^{-2}$ at 773 K by introducing 0.50% In.

3.4 Thermal transport properties of polycrystalline $Sn_{0.98x}Na_{0.02}In_xSe$

Figure 5a shows the total thermal conductivity of $Sn_{0.98-x}Na_{0.02}In_xSe$. It can be seen that the total thermal conductivity gradually decreases with temperature increasing. The total thermal conductivity is determined by the following equation:

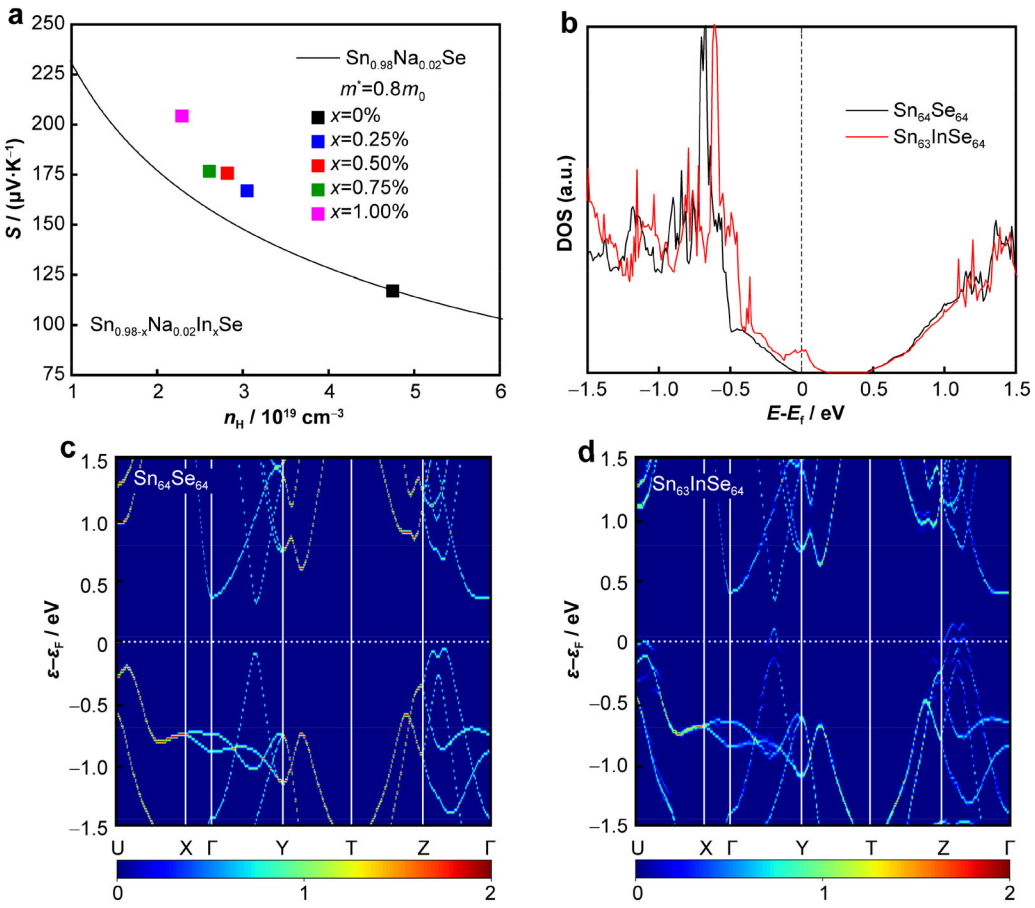

Fig. 4 **a** Pisarenko relationship of $Sn_{0.98-x}Na_{0.02}In_xSe$ at room temperature; **b** comparison of density of state (DOS) for undoped SnSe (black line) and In-doped SnSe (red line), where vertical line denotes Fermi level; **c** electronic band structures of $Sn_{64}Se_{64}$; **d** electronic band structures of $Sn_{63}InSe_{64}$

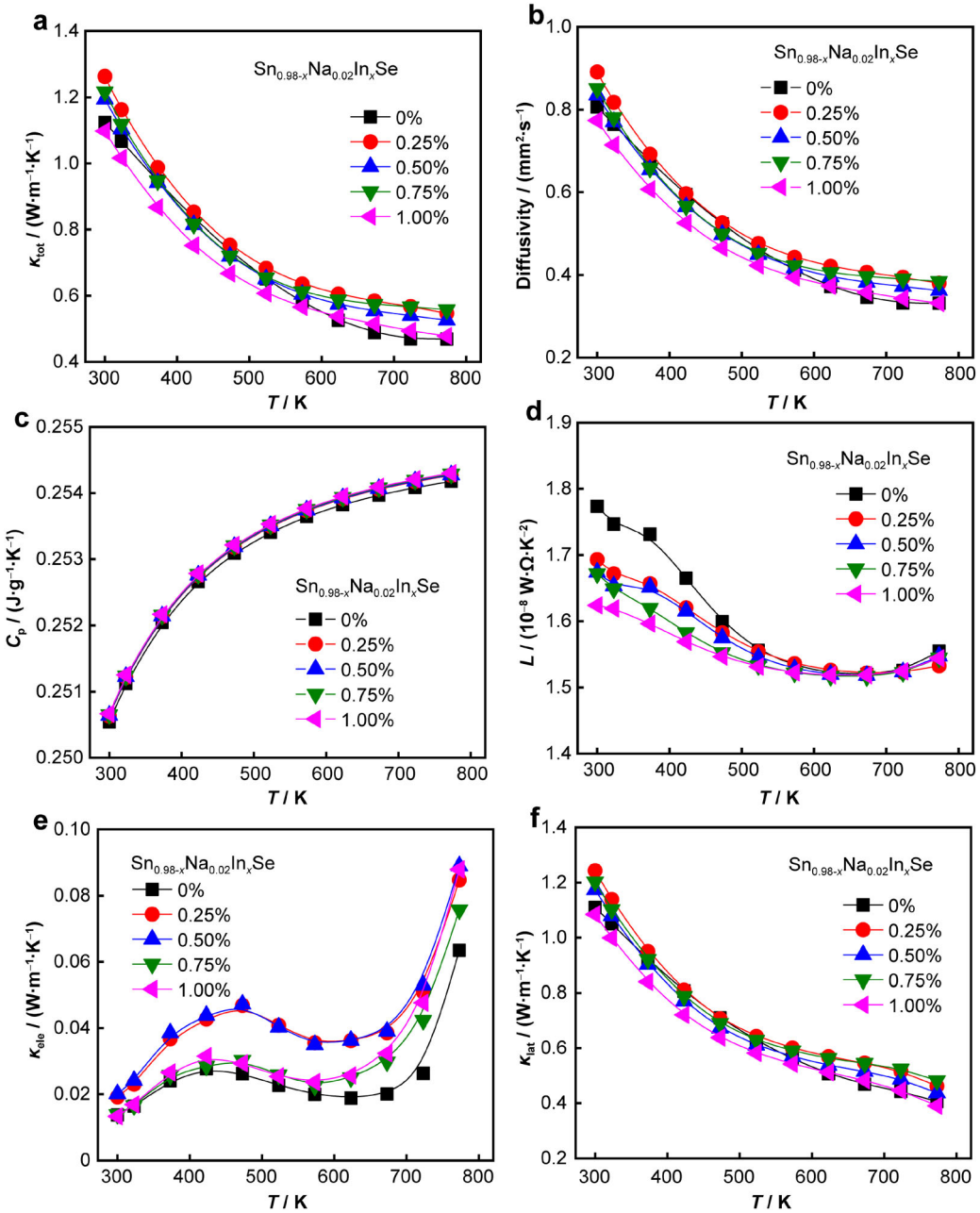

Fig. 5 Thermal transport properties of $Sn_{0.98-x}Na_{0.02}In_xSe$ samples with rising temperature: **a** total thermal conductivity; **b** thermal diffusivity; **c** specific heat; **d** Lorenz number; **e** electronic thermal conductivity; **f** lattice thermal conductivity

$$\kappa_{tot} = DC_p\rho \quad (6)$$

where ρ is the sample density, as listed in Table S1; D is the thermal diffusion coefficient measured by the laser thermal conductivity meter LFA, and C_p is the specific heat calculated by the Debye model, as shown in Fig. 5b, c. Doping In slightly increases the total thermal conductivity. Specifically, the room-temperature total thermal conductivity rises from ~ 1.12 to ~ 1.26 W·m^{-1}·K^{-1}, and high-temperature values range from ~ 0.47 to ~ 0.55 W·m^{-1}·K^{-1} at 773 K. There is no quantitative relationship between the lattice thermal conductivity and the carriers, and it is a relatively independent parameter, which can be determined by the following equation:

$$\kappa_{lat} = \kappa_{tot} - \kappa_{ele} \quad (7)$$

According to the Wiedemann–Franz law, the relationship of κ_{ele} is as follows:

$$\kappa_{ele} = L\sigma T = Ln e \mu T \quad (8)$$

where L is the Lorentz number, which is obtained by fitting multiple Seebeck coefficients at different temperatures and

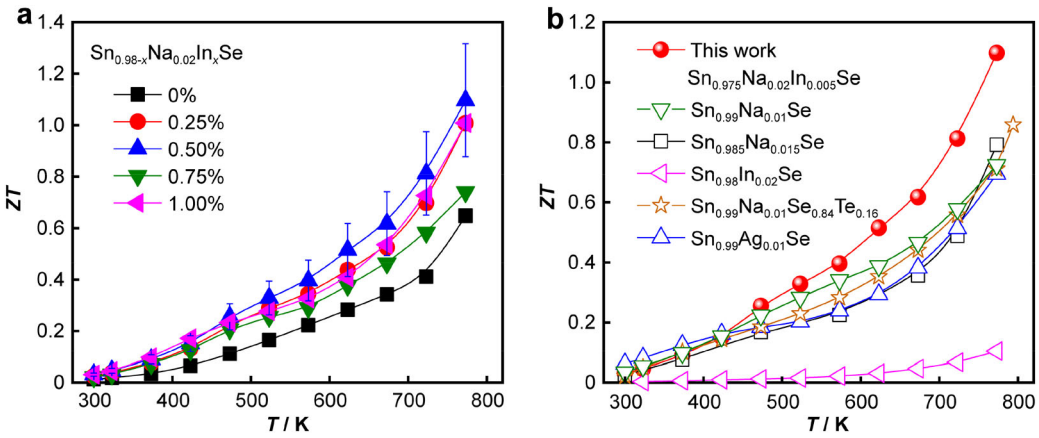

Fig. 6 *ZT* values for p-type SnSe polycrystalline thermoelectrics: **a** *ZT* values as a function of temperature for In-doped polycrystalline SnSe; **b** comparisons for *ZT* values in $Sn_{0.975}Na_{0.02}In_{0.005}Se$ of this work and reported $Sn_{0.99}Ag_{0.01}Se$ [15], $Sn_{0.99}Na_{0.01}Se_{0.84}Te_{0.16}$ [42], $Sn_{0.985}Na_{0.015}Se$ [57], $Sn_{0.98}Na_{0.01}Se$ [17] and$Sn_{0.98}In_{0.02}Se$ [38]

is mainly used to estimate the reduced chemical potential, as shown in Fig. 5d. Figure 5e shows the electronic thermal conductivity of $Sn_{0.98-x}Na_{0.02}In_xSe$ polycrystalline samples. From Eq. (8), κ_{ele} is determined by the carrier concentration and carrier mobility. Therefore, κ_{ele} shows an increasing trend with In doping, as shown in Fig. 5e. Figure 5f shows the κ_{lat} of $Sn_{0.98-x}Na_{0.02}In_xSe$ samples as a function of temperature, from which we can see no obvious change with In doping. This also indicates that the increase of total thermal conductivity mainly arises from the electronic part.

3.5 Figure of merit (*ZT*) for polycrystalline $Sn_{0.98-x}Na_{0.02}In_xSe$

The thermoelectric figure of merit (*ZT*) with In doping samples is shown in Fig. 6a. With the optimized electrical transport properties and maintained thermal part, the final *ZT* values demonstrate significant enhancement with In doping. Specifically, the maximum *ZT* value for each sample ranges from $\sim$ 0.6 for $Sn_{0.98}Na_{0.02}Se$ to $\sim$ 1.1 for $Sn_{0.975}Na_{0.02}In_{0.005}Se$ at 773 K, indicating a 72% increase with 0.50% In doping. Furthermore, we compare the optimized *ZT* of this work with the previously reported p-type SnSe polycrystalline systems with similar experimental routes, as shown in Fig. 6b. The comparison indicates that upon Na doping, further In doping has a significant effect on optimizing the thermoelectric performance of p-type polycrystalline SnSe by producing resonant effect.

4 Conclusion

In this work, we first compared the electrical conductivity between p-type crystalline and polycrystalline SnSe to estimate the three-stage curve for polycrystalline sample. This feature mainly arises from the various dominating phonon scattering mechanisms, which change from grain boundary scattering to acoustic phonon scattering with rising temperature and can be further verified by microstructure characterization and theoretically calculated simulation. To further improve the electrical transport properties of polycrystalline SnSe, we synthesized $Sn_{0.98-x}Na_{0.02}In_xSe$ samples by melting and SPS method. It is found that In doping can induce the resonant effect of electronic states, which increases the density of states near Fermi level and strengthens the effective mass, resulting in an $\sim$ 50% enhancement of the Seebeck coefficient. the electrical conductivity was also optimized by carrier concentration and carrier mobility modification via In doping, leading to greatly enhanced power factors over a wide temperature range. Furthermore, while In doping further optimizes the electrical transport properties, it has no negative effects on the thermal transports, which contributes to significant improvements on the final *ZT* values, and the maximum *ZT* value of 0.50%In-doped sample exceeds 1.1, while that of In-free sample is $\sim$ 0.6. The present results elucidate that the resonant effects can be successfully implemented in polycrystalline SnSe systems for thermoelectric optimization and the performance might be further enhanced upon this by modifying the carrier mobility via microstructure engineering.

Acknowledgements This work was financially supported by the National Key Research and Development Program of China (Nos. 2018YFA0702100 and 2018YFB0703600), the National Natural Science Foundation of China (Nos. 51772012 and 51671015), Beijing Natural Science Foundation (No. JQ18004), and National Postdoctoral Program for Innovative Talents (No. BX20200028). L.D.Z. thanks for the support from the National Science Fund for Distinguished Young Scholars (No. 51925101) and the high performance computing (HPC) resources at Beihang University.

References

[1] Snyder GJ, Toberer ES. Complex thermoelectric materials. Nat Mater. 2008;7(2):105.

[2] Sootsman JR, Chung DY, Kanatzidis MG. New and old concepts in thermoelectric materials. Angew Chem Int Ed. 2009; 48(46):8616–39.

[3] Tan G, Zhao LD, Kanatzidis MG. Rationally designing high-performance bulk thermoelectric materials. Chem Rev. 2016;116(16):12123.

[4] Zhang X, Zhao LD. Thermoelectric materials: energy conversion between heat and electricity. J Mater. 2015;1(2):92.

[5] Biswas K, He JQ, Blum ID, Wu CI, Hogan TP, Seidman DN, Dravid VP, Kanatzidis MG. High-performance bulk thermoelectrics with all-scale hierarchical architectures. Nat. 2012; 489(7416):414.

[6] Heremans JP, Jovovic V, Toberer ES, Saramat A, Kurosaki K, Charoenphakdee A, Yamanaka S, Snyder GJ. Enhancement of thermoelectric efficiency in PbTe by distortion of the electronic density of states. Sci. 2008;321(5888):554.

[7] Zhang H, Li JT, Ding FZ, Qu F, Li H, Gu HW. Combustion synthesis of ZrNiSn half-Heusler thermoelectric materials. Chin J Rare Met. 2019;43(4):337.

[8] Pei YZ, Shi XY, LaLonde A, Wang H, Chen LD, Snyder GJ. Convergence of electronic bands for high performance bulk thermoelectrics. Nat. 2011;473(7345):66.

[9] Rahnamaye Aliabad HA, Sabazadeh Z, Abareshi A. Electronic structure and thermal properties of bulk and nano-layer of $TAlO_2$ (T=Cu, Ag and Au) delafossite oxides. Rare Met. 2019; 38(10):905.

[10] Zhao LD, Wu HJ, Hao SQ, Wu CI, Zhou XY, Biswas K, He JQ, Hogan TP, Uher C, Wolverton C, Dravid VP, Kanatzidis MG. All-scale hierarchical thermoelectrics: MgTe in PbTe facilitates valence band convergence and suppresses bipolar thermal transport for high performance. Energy Environ Sci. 2013;6(11): 3346.

[11] Zhang X, Wang DY, Wu HJ, Yin MJ, Pei YL, Gong SK, Huang L, Pennycook SJ, He JQ, Zhao LD. Simultaneously enhancing the power factor and reducing the thermal conductivity of SnTe via introducing its analogues. Energy Environ Sci. 2017;10(11): 2420.

[12] Xiao Y, Wu HJ, Cui J, Wang DY, Fu LW, Zhang Y, Chen Y, He JQ, Pennycook SJ, Zhao LD. Realizing high performance n-type PbTe by synergistically optimizing effective mass and carrier mobility and suppressing bipolar thermal conductivity, energy environ. Sci. 2018;11(9):2486.

[13] Qin BC, Xiao Y, Zhou YM, Zhao LD. Thermoelectric transport properties of Pb-Sn-Te-Se system. Rare Met. 2018;37(4):343.

[14] Qu WW, Zhang XX, Yuan BF, Zhao LD. Homologous layered $InFeO_3(ZnO)_m$: new promising abradable seal coating materials. Rare Met. 2018;37(2):79.

[15] Chen CL, Wang H, Chen YY, Day T, Snyder GJ. Thermoelectric properties of p-type polycrystalline SnSe doped with Ag. J Mater Chem A. 2014;2(29):11171.

[16] Li JC, Li D, Qin XY, Zhang J. Enhanced thermoelectric performance of p-type SnSe doped with Zn. Scr Mater. 2017;126:6.

[17] Wei TR, Tan GJ, Zhang XM, Wu CF, Li JF, Dravid VP, Snyder GJ, Kanatzidis MG. Distinct impact of alkali-ion doping on electrical transport properties of thermoelectric p-type polycrystalline SnSe. J Am Chem Soc. 2016;138(28):8875.

[18] Wu D, Pei YL, Wang Z, Wu HJ, Huang L, Zhao LD, He JQ. Significantly enhanced thermoelectric performance in n-type heterogeneous BiAgSeS composites. Adv Funct Mater. 2014; 24(48):7763.

[19] Xiao Y, Zhao LD. Charge and phonon transport in PbTe-based thermoelectric materials. npj Quantum Mater. 2018;3(1):1.

[20] Tan GJ, Zhao LD, Shi FY, Doak JW, Lo SH, Sun H, Wolverton C, Dravid VP, Uher C, Kanatzidis MG. High thermoelectric performance of p-type SnTe via a synergistic band engineering and nanostructuring approach. J Am Chem Soc. 2014;136(19): 7006–17.

[21] Ge ZH, Song DS, Chong XY, Zheng FS, Jin L, Qian X, Zheng L, Dunin-Borkowski RE, Qin P, Feng J, Zhao LD. Boosting the thermoelectric performance of (Na, K)-codoped polycrystalline SnSe by synergistic tailoring of the band structure and atomic-scale defect phonon scattering. J Am Chem Soc. 2017; 139(28):9714.

[22] Tan GJ, Shi FY, Hao SQ, Chi H, Zhao LD, Uher C, Wolverton C, Dravid VP, Kanatzidis MG. Codoping in SnTe: enhancement of thermoelectric performance through synergy of resonance levels and band convergence. J Am Chem Soc. 2015;137(15): 5100.

[23] Zhao WY, Liu ZY, Wei P, Zhang QJ, Zhu WT, Su XL, Tang XF, Yang JH, Liu Y, Shi J, Chao YM, Lin SQ, Pei YZ. Magnetoelectric interaction and transport behaviours in magnetic nanocomposite thermoelectric materials. Nat Nanotechnol. 2017;12(1):55.

[24] Xiao Y, Chang C, Pei YL, Wu D, Peng KL, Zhou XY, Gong SK, He JQ, Zhang YS, Zeng Z, Zhao LD. Origin of low thermal conductivity in SnSe. Phys Rev B. 2016;94(12):125203.

[25] Chang C, Zhao LD. Anharmoncity and low thermal conductivity in thermoelectrics. Mater Today Phys. 2018;4:50.

[26] Liu HL, Shi X, Xu FF, Zhang LL, Zhang WQ, Chen LD, Li Q, Uher C, Day T, Snyder GJ. Copper ion liquid-like thermoelectrics. Nat Mater. 2012;11(5):422.

[27] Pei YL, Chang C, Wang Z, Yin MJ, Wu MH, Tan GJ, Wu HJ, Chen YX, Zheng L, Gong SK, Zhu TJ, Zhao XB, Huang L, He JQ, Kanatzidis MG, Zhao LD. Multiple converged conduction bands in $K_2Bi_8Se_{13}$: a promising thermoelectric material with extremely low thermal conductivity. J Am Chem Soc. 2016; 138(50):16364.

[28] Wang DY, Huang ZW, Zhang Y, Hao LJ, Wang GT, Deng SH, Wang HL, Chen J, He LH, Xiao B, Xu YD, Pennycook SJ, Wu HJ, Zhao LD. Extremely low thermal conductivity from bismuth selenohalides with 1D soft crystal structure. Sci China Mater. 2020;63(9):1759.

[29] Zhou YM, Zhao LD. Promising thermoelectric bulk materials with 2D structures. Adv Mater. 2017;29(45):1702676.

[30] Zhao LD, Lo SH, Zhang YS, Sun H, Tan GJ, Uher C, Wolverton C, Dravid VP, Kanatzidis MG. Ultralow thermal conductivity and high thermoelectric figure of merit in SnSe crystals. Nat. 2014;508(7496):373.

[31] Zhao LD, Tan GJ, Hao SQ, He JQ, Pei YL, Chi H, Wang H, Gong SK, Xu HB, Dravid VP, Uher C, Snyder GJ, Wolverton C, Kanatzidis MG. Ultrahigh power factor and thermoelectric performance in hole-doped single-crystal SnSe. Sci. 2016; 351(6269):141.

[32] Qin BC, Zhang Y, Wang DY, Zhao Q, Gu BC, Wu HJ, Zhang HJ, Ye BJ, Pennycook SJ, Zhao LD. Ultrahigh average *ZT* realized in p-type SnSe crystalline thermoelectrics through producing extrinsic vacancies. J Am Chem Soc. 2020;142(12): 5901.

[33] Qin BC, Wang DY, He WK, Zhang Y, Wu HJ, Pennycook SJ, Zhao LD. Realizing high thermoelectric performance in p-type SnSe through crystal structure modification. J Am Chem Soc. 2019;141(2):1141.

[34] Chang C, Wu MH, He DS, Pei YL, Wu CF, Wu XF, Yu HL, Zhu FY, Wang KD, Chen Y, Huang L, Li JF, He JQ, Zhao LD. 3D charge and 2D phonon transports leading to high out-of-plane ZT in n-type SnSe crystals. Sci. 2018;360(6390):778.

[35] Chang C, Wang DY, He DS, He WK, Zhu FY, Wang GT, He JQ, Zhao LD. Realizing high-ranged out-of-plane *ZT*s in n-type SnSe crystals through promoting continuous phase transition. Adv Energy Mater. 2019;9(28):1901334.
[36] Zhao Q, Wang DY, Qin BC, Wang GT, Qiu YT, Zhao LD. Synergistically optimized electrical and thermal transport properties of polycrystalline SnSe via alloying SnS. J Solid State Chem. 2019;273:85.
[37] Zhao Q, Qin BC, Wang DY, Qiu YT, Zhao LD. Realizing high thermoelectric performance in polycrystalline SnSe via silver doping and germanium alloying. ACS Appl Energy Mater. 2020; 3(3):2049.
[38] Singh NK, Bathula S, Gahtori B, Tyagi K, Haranath D, Dhar A. The effect of doping on thermoelectric performance of p-type SnSe: promising thermoelectric material. J Alloy Compd. 2016; 668:152.
[39] Chen YX, Ge ZH, Yin MJ, Feng D, Huang XQ, Zhao WY, He JQ. Understanding of the extremely low thermal conductivity in high-performance polycrystalline SnSe through potassium doping. Adv Funct Mater. 2016;26(37):6836.
[40] Peng KL, Lu X, Zhan H, Hui S, Tang XD, Wang GW, Dai JY, Uher C, Wang GY, Zhou XY. Broad temperature plateau for high *ZT*s in heavily doped p-type SnSe single crystals. Energy Environ Sci. 2016;9(2):454.
[41] Zhang JH, Xu JT, Tan XJ, Wang HX, Liu GQ, Shao HZ, Yu B, Yue S, Jiang J. Optimized orientation and enhanced thermoelectric performance in $Sn_{0.97}Na_{0.03}Se$ with Te addition. J Mater Chem C. 2019;7(9):2653.
[42] Wei TR, Wu CF, Zhang XZ, Tan Q, Sun L, Pan Y, Li JF. Thermoelectric transport properties of pristine and Na-doped $SnSe_{1-x}Te_x$ polycrystals. Phys Chem Chem Phys. 2015;17(44): 30102.
[43] Liang S, Xu J, Noudem JG, Wang H, Tan X, Liu GQ, Shao H, Yu B, Yue S, Jiang J. Thermoelectric properties of textured polycrystalline $Na_{0.03}Sn_{0.97}Se$ enhanced by hot deformation. J Mater Chem A. 2018;6(46):23730.
[44] Peng KL, Wu H, Yan YC, Guo LJ, Wang GY, Lu X, Zhou XY. Grain size optimization for high-performance polycrystalline SnSe thermoelectrics. J Mater Chem A. 2017;5(27):14053.
[45] Xiao Y, Wu HJ, Wang DY, Niu CL, Pei YL, Zhang Y, Spanopoulos I, Witting IT, Li X, Pennycook SJ, Snyder GJ, Kanatzidis MG, Zhao LD. Amphoteric indium enables carrier engineering to enhance the power factor and thermoelectric performance in n-type $Ag_nPb_{100}InnTe_{100+2n}$(LIST). Adv Energy Mater. 2019;9(17):1900414.
[46] Zhang Q, Liao BL, Lan YC, Lukas K, Liu WS, Esfarjani K, Opeil C, Broido D, Chen G, Ren ZF. High thermoelectric performance by resonant dopant indium in nanostructured SnTe. Proc Natl Acad Sci U S A. 2013;110(33):13261.
[47] Mao J, Wu YX, Song SW, Shuai J, Liu ZH, Pei YZ, Ren ZF. Anomalous electrical conductivity of n-type Te-doped $Mg_{3.2}Sb_{1.5}Bi_{0.5}$. Mater Today Phys. 2017;3:1.
[48] Mao J, Wu YX, Song SW, Zhu Q, Shuai J, Liu ZH, Pei YZ, Ren ZF. Defect engineering for realizing high thermoelectric performance in n-type Mg_3Sb_2-based materials. ACS Energy Lett. 2017;2(10):2245.
[49] Wang S, Hui S, Peng KL, Bailey TP, Zhou XY, Tang XF, Uher C. Grain boundary scattering effects on mobilities in p-type polycrystalline SnSe. J Mater Chem C. 2017;5(39):10191.
[50] Levinson J, Shepherd FR, Scanlon PJ, Westwood WD, Rider M. Conductivity behavior in polycrystalline semiconductor thin film transistors. J Appl Phys. 1982;53(2):1193.
[51] Seto JYW. The electrical properties of polycrystalline silicon films. J Appl Phys. 1975;46(12):5247.
[52] Kuo JJ, Kang SD, Imasato K, Tamaki H, Ohno S, Kanno T, Snyder GJ. Grain boundary dominated charge transport in Mg_3Sb_2-based compounds. Energy Environ Sci. 2018;11(2):429.
[53] Slade TJ, Grovogui JA, Kuo JJ, Anand S, Bailey TP, Wood M, Uher C, Snyder GJ, Dravid VP, Kanatzidis MG. Understanding the thermally activated charge transport in $NaPb_{(m)}SbQ_{(m+2)}$ (Q = S, Se, Te) thermoelectrics: weak dielectric screening leads to grain boundary dominated charge carrier scattering. Energy Environ Sci. 2020;13(5):1509.
[54] Schnering HGV, Wiedemeier H. The high temperature structure of β-SnS and β-SnSe and the B16-to-B33 type λ-transition path. Z fur Krist. 1981;156:143.
[55] Serraon-Sanchez F, Nemes NM, Dura OJ, Fernandez-Diaz MT, Martinez JL, Alonso JA. Structural phase transition in polycrystalline SnSe: a neutron diffraction study in correlation with thermoelectric properties. J Appl Crystallogr. 2016;49:2138.
[56] Sist M, Zhang JW, Iversen BB. Crystal structure and phase transition of thermoelectric SnSe. Acta Crystallogr Sect B: Struct Sci Cryst Eng Mater. 2016;72(3):310.
[57] Chere EK, Zhang Q, Dahal K, Cao F, Mao J, Ren ZF. Studies on thermoelectric figure of merit of Na-doped p-type polycrystalline SnSe. J Mater Chem A. 2016;4(5):1848.